AAEC/E357

AUSTRALIAN ATOMIC ENERGY COMMISSION

RESEARCH ESTABLISHMENT

LUCAS HEIGHTS

CORRELATION AND FLUX TILT MEASUREMENTS OF COUPLED-CORE REACTOR ASSEMBLIES

by

J. R. HARRIES

January 1976

ISBN 0 642 99728 4

AUSTRALIAN ATOMIC ENERGY COMMISSION
RESEARCH ESTABLISHMENT
LUCAS HEIGHTS

CORRELATION AND FLUX TILT MEASUREMENTS OF COUPLED-CORE REACTOR ASSEMBLIES

by

J.R. HARRIES

ABSTRACT

The systematics of coupling reactivity and time delay between cores have been investigated with a series of coupled-core assemblies on the AAEC Split-table Critical Facility. The assemblies were similar to the Universities' Training Reactor (UTR), but had graphite coupling region thickness of 450 mm, 600 mm and 800 mm. The coupling reactivity measured by both the cross-correlation of reactor noise and the flux tilt methods was stronger than for the UTRs, but showed a similar trend with core spacing.

The cross-correlograms were analysed using the two-node model to derive the time delays between the cores. The time delays were compared with thermal neutron wave propagation, and found to be consistent when the time delays were added to the individual node response-function delays.

National Library of Australia card number and ISBN 0 642 99728 4

The following descriptors have been selected from the INIS Thesaurus to describe the subject content of this report for information retrieval purposes. For further details please refer to IAEA–INIS–12 (INIS: Manual for Indexing) and IAEA–INIS–13 (INIS: Thesaurus) published in Vienna by the International Atomic Energy Agency.

CORRELATION FUNCTIONS; COUPLED REACTOR CORES; GRAPHITE; MOATA REACTOR; NEUTRON FLUX TILTING; REACTIVITY; REACTOR KINETICS; REACTOR NOISE; ROD DROP METHOD; THERMAL NEUTRONS; TIME DEPENDENCE

CONTENTS

		Page
1.	INTRODUCTION	1
2.	THEORETICAL BACKGROUND	1
3.	EXPERIMENTAL METHOD	5
4.	REACTOR ASSEMBLIES	7
5.	CORRELATION RESULTS	8
6.	FLUX TILT	11
7.	DISCUSSION	14
	7.1 Coupling Reactivity	14
	7.2 Time Delay between the Cores	17
8.	CONCLUSION	20
9.	ACKNOWLEDGEMENTS	20
10.	REFERENCES	20

Figure 1 Theoretical cross-correlation functions for a coupled-core reactor with various time delays between cores

Figure 2 Auto- and cross-correlation functions for a delay of 4 ms between cores
(a) without flux tilting (b) with flux tilting

Figure 3 Correlogram window function for 0.666 ms correlograms

Figure 4(a) Top view of assembly M1, with 450 mm coupling region

Figure 4(b) Front view of assembly M1 showing the correlation detector positions

Figure 5 Flux scans across assembly M3 at a height of 700 mm for two different control rod configurations

Figure 6 Cross-correlograms for assemblies M1, M2 and M3 scaled to have the same exponential asymptotes

Figure 7 Plots of both the sum and difference of auto- and cross-correlograms for an experiment on assembly M3. The least squares fits to an exponential function are shown. A background component has been subtracted

Figure 8 Experimental correlograms from assembly M3 showing the effect of a flux tilt

Figure 9(a) Cross-spectrum components for experiment 6, assembly M3 showing the two-node fit (unbroken line) to the experimental data points

CONTENTS(Continued)

Figure 9(b) Cross-spectrum components at higher frequencies (experimental points as dots) showing the sink frequency at 203 rad s^{-1}. The line is the theoretical two-node model fit to the data

Figure 10 Coupling reactivities of the AAEC assemblies compared with the results for other graphite coupled reactors

1. INTRODUCTION

Coupled-core reactors can show a strong space dependence in their kinetic behaviour and large flux tilts can be produced. A knowledge of the kinetic behaviour of such coupled-core reactors aids in the understanding of the more complex space-dependent kinetic response of large power reactors.

The present series of experiments was carried out on the AAEC Splittable Critical Facility. The basic assembly was a mockup of the AAEC Moata reactor, a water moderated and cooled, graphite reflected, UTR-10 reactor with a 457 mm graphite coupling region between the two core tanks. In the mockup assemblies, the water was simulated by polythene, but the hydrogen-to-fuel ratio was approximately equal to that of Moata. Assemblies were constructed with graphite coupling region thicknesses of 450 mm, 600 mm and 800 mm.

The coupled-core effects were determined from the correlation function of the neutron density fluctuations in each core, and by measuring the neutron flux tilt for a given reactivity change. The correlation experiment measures directly the space-dependence of the prompt neutron chain reaction.

2. THEORETICAL BACKGROUND

Theories for the kinetic behaviour of coupled-core reactors can be derived from a two-node model [Baldwin 1959, Albrecht & Seifritz 1968], or by modal analysis of the neutron flux [Danofsky 1969, Rydin *et al.* 1971, Ebert & Gallaher 1971]. The two-node one-energy group model will be used for the analysis of the present experiment because it lends itself more readily to physical interpretation.

The two-node, one-group kinetics equations for core 1 are:

$$\frac{dN_1(t)}{dt} = \frac{\rho_1-\beta}{\Lambda_1} N_1(t) + \frac{\varepsilon}{\Lambda_1}\int_0^\infty P(\tau)N_2(t-\tau)d\tau + \Sigma\lambda_i C_{i_1}(t) + S_1(t) \quad ,$$

$$\frac{dC_{i_1}(t)}{dt} = \frac{\beta_i}{\Lambda_1} N_1(t) - \lambda_i C_{i_1}(t) \quad , \qquad \ldots(1)$$

where $N_1(t)$ and $N_2(t)$ are the fundamental mode amplitudes for the neutron densities in each core, ε is the coupling coefficient, $P(t)$ is the delay

function for neutrons travelling from one core to the other, and ρ_i and Λ_i are the reactivity and prompt neutron generation time of core i. Now the neutron density amplitudes and sources can be divided into a steady component and a variable component such that the mean $\langle n_1(t)\rangle = 0$, *i.e.*

$N_1(t) = \langle N_1\rangle + n_1(t)$, etc.

In a critical reactor, the steady-state values give:

$$\varepsilon^2 = \rho_1\rho_2 \quad ,$$

$$\varepsilon\langle N_2\rangle = -\rho_1\langle N_1\rangle \quad ,$$

$$\langle N_1\rangle/\langle N_2\rangle = \sqrt{\rho_2/\rho_1} \quad . \qquad \ldots(2)$$

The frequencies of interest in the correlation experiments are greater than the delayed neutron decay constants, so the delayed neutron term $\Sigma\lambda_i C_i$ can be considered part of the source terms. After substitution, and using the mean conditions to eliminate the time invariant components, two equations in the fluctuation amplitudes are obtained:

$$\frac{dn_1(t)}{dt} = \frac{\rho_1-\beta}{\Lambda_1} n_1(t) + \frac{\varepsilon}{\Lambda_1}\int_0^\infty P(\tau)n_2(t-\tau)d\tau + s_1(t) \quad ,$$

$$\frac{dn_2(t)}{dt} = \frac{\rho_2-\beta}{\Lambda_2} n_2(t) + \frac{\varepsilon}{\Lambda_2}\int_0^\infty P(\tau)n_1(t-\tau)d\tau + s_2(t) \quad . \qquad \ldots(3)$$

The Laplace transform solution of these equations, with $\Lambda_1 = \Lambda_2 = \Lambda$, is

$$\bar{n}_1(\omega) = \frac{(\varepsilon/\Lambda)\bar{p}(\omega)\bar{s}_2(\omega) + [i\omega + (\beta-\rho_2)/\Lambda]\bar{s}_1(\omega)}{[i\omega + (\beta-\rho_1)/\Lambda]\,[i\omega + (\beta-\rho_2)/\Lambda] - (\varepsilon/\Lambda)^2\bar{p}^2(\omega)}$$

$$\bar{n}_2(\omega) = \frac{(\varepsilon/\Lambda)\bar{p}(\omega)\bar{s}_1(\omega) + [i\omega + (\beta-\rho_1)/\Lambda]\bar{s}_2(\omega)}{[i\omega + (\beta-\rho_1)/\Lambda]\,[i\omega + (\beta-\rho_2)/\Lambda] - (\varepsilon/\Lambda)^2\bar{p}^2(\omega)} \qquad \ldots(4)$$

where the 'bar' symbol indicates a transformed variable.

The auto- and cross-spectra are obtained by multiplying the two functions together and taking the time average. The two source terms are uncorrelated, hence the time averages of their cross-powers are zero [*i.e.* $\langle\bar{s}_1(\omega)\bar{s}_2^*(\omega)\rangle = \langle\bar{s}_2(\omega)\bar{s}_1^*(\omega)\rangle = 0$] and only the auto-powers contribute [*i.e.* $\langle\bar{s}_1(\omega)\bar{s}_1^*(\omega)\rangle = |\bar{s}_1|^2$, $\langle\bar{s}_2(\omega)\bar{s}_2^*(\omega)\rangle = |\bar{s}_2|^2$].

The spectral density of the source component is independent of frequency. Hence the cross- and auto-spectral densities of the neutron distribution functions ($S_{12}(\omega)$ and $S_{11}(\omega)$ respectively) in each core to the random source variations are:

$$S_{12}(\omega) = \langle\bar{n}_1(\omega)\bar{n}_2^*(\omega)\rangle =$$

$$\frac{(\varepsilon/\Lambda)\bar{p}(\omega)[-i\omega + (\beta-\rho_1)/\Lambda]|\bar{s}_2|^2 + (\varepsilon/\Lambda)\bar{p}^*(\omega)[i\omega + (\beta-\rho_2)/\Lambda]|\bar{s}_1|^2}{|[i\omega + (\beta-\rho_1)/\Lambda][i\omega + (\beta-\rho_2)/\Lambda] - (\varepsilon/\Lambda)^2\bar{p}^2(\omega)|^2} \quad ,$$

$$S_{11}(\omega) = \langle\bar{n}_1(\omega)\bar{n}_1^*(\omega)\rangle =$$

$$\frac{(\varepsilon/\Lambda)^2|\bar{p}(\omega)|^2|\bar{s}_2|^2 + [\omega^2 + (\beta-\rho_2)/\Lambda]|\bar{s}_1|^2}{|[i\omega + (\beta-\rho_1)/\Lambda][i\omega + (\beta-\rho_2)/\Lambda] - (\varepsilon/\Lambda)^2\bar{p}^2(\omega)|^2} \quad . \qquad \ldots(5)$$

In the current experiment, the data could be explained by assuming that all the coupling neutrons had the same time delay, t_d, *i.e.* $p(t) = \delta(t-t_d)$ and $\bar{p}(\omega) = \exp(-i\omega t_d)$. Substituting into Equation (5) gives the following real and imaginary components:

$$R\{S_{12}(\omega)\} = \frac{1}{D}\{[|\bar{s}_1|^2(\beta-\rho_2)/\Lambda + |\bar{s}_2|^2(\beta-\rho_1)/\Lambda]\cos\omega t_d -$$

$$- \omega[|\bar{s}_1|^2 + |\bar{s}_2|^2]\sin\omega t_d \} \quad ,$$

$$I\{S_{12}(\omega)\} = \frac{1}{D}\{[|\bar{s}_1|^2(\beta-\rho_2)/\Lambda - |\bar{s}_2|^2(\beta-\rho_1)/\Lambda]\sin\omega t_d +$$

$$+ \omega[|\bar{s}_1|^2 - |\bar{s}_2|^2]\cos\omega t_d \} \quad , \qquad \ldots(6)$$

where D is the same denominator as before. These equations show that the imaginary component will be zero if the reactor is symmetric, *i.e.* if

the reactivities and flux levels are the same in each core. The real component will be zero at the frequency ('sink frequency') when the following condition is satisfied:

$$\omega \tan \omega t_d = \frac{|\bar{s}_1|^2 (\beta-\rho_2)/\Lambda + |\bar{s}_2|^2 (\beta-\rho_1)/\Lambda}{|\bar{s}_1|^2 + |\bar{s}_2|^2} \quad . \qquad \ldots(7)$$

In a symmetric reactor, the spectral power density will be zero at the sink frequency.

The correlation functions are calculated by Fourier transforming the cross- and auto-spectra. The essential features of the correlation functions can be shown by assuming that there is no time delay between the cores, $t_d = 0$, and that the reactor is symmetrical. In that case, the Fourier transform of the spectral densities gives the auto-correlation ($R_{11}(\tau)$) and the cross-correlation ($R_{12}(\tau)$):

$$R_{11}(\tau) = \frac{|\bar{s}|^2}{2} \sqrt{\frac{\pi}{2}} \left\{ \frac{\exp[-(\beta-\rho-\varepsilon)|\tau|/\Lambda]}{(\beta-\rho-\varepsilon)/\Lambda} + \frac{\exp[-(\beta-\rho+\varepsilon)|\tau|/\Lambda]}{(\beta-\rho+\varepsilon)/\Lambda} \right\}$$

$$R_{12}(\tau) = \frac{|\bar{s}|^2}{2} \sqrt{\frac{\pi}{2}} \left\{ \frac{\exp[-(\beta-\rho-\varepsilon)|\tau|/\Lambda]}{(\beta-\rho-\varepsilon)/\Lambda} - \frac{\exp[-(\beta-\rho+\varepsilon)|\tau|/\Lambda]}{(\beta-\rho+\varepsilon)/\Lambda} \right\}$$

$\ldots(8)$

For a critical and symmetrical reactor with no external neutron source, $\rho_1 = \rho_2 = -\varepsilon$ from Equation (1).

A neutron detector cannot measure the fundamental neutron mode amplitude exactly as this would require all the neutrons to be detected and returned to the system. The detector output consists of a signal proportional to the fundamental amplitude, and a random noise component which is uncorrelated in the two detectors and so does not contribute to the cross-correlation function. However, the noise component will produce a peak in the auto-correlation function at zero time lag. Hence the correlation functions observed in a critical reactor will have the form:

$$R_{11}(\tau) \propto \frac{\exp(-\beta|\tau|/\Lambda)}{\beta/\Lambda} + \frac{\exp[-(\beta+2\varepsilon)|\tau|/\Lambda]}{(\beta+2\varepsilon)/\Lambda} + k\delta(\tau)$$

$$R_{12}(\tau) \propto \frac{\exp(-\beta|\tau|/\Lambda)}{\beta/\Lambda} - \frac{\exp[-(\beta+2\varepsilon)|\tau|/\Lambda)}{(\beta+2\varepsilon)/\Lambda} \qquad \ldots(9)$$

The correlation functions are made up of two exponential components, one characteristic of the reactor as a whole with decay constant $\alpha = \beta/\Lambda$, and the other depending on the coupling and with a decay constant of $(\beta+2\varepsilon)/\Lambda$.

The theoretical cross-correlation functions for various time delays have been calculated from Equation (6) and the results are shown in Figure 1 for a symmetric reactor. The values of α and ε used are similar to those of the assembly M3. The time delay produces a minimum in the cross-correlation functions near zero time lag.

The effect of flux tilt on the correlation functions is shown in Figure 2. When a flux tilt is present, the cross-correlation function is not symmetric and the relative amplitudes of the auto-correlation functions are approximately proportional to the square of the flux in each core. The flux tilt parameter, T, is defined as N_1/N_2, where N_1 and N_2 are the amplitudes of the neutron density functions in each core.

Albrecht & Seifritz [1968] used the coherence function (the ratio of the cross-spectral density to the geometric mean of the two auto-spectral densities) to describe the properties of coupled-core reactors. This approach suffers from the difficulty of measuring the auto-spectral density at high frequencies in the presence of white noise. The auto-spectral density depends on the coupling (Equation 5) and so cannot be readily extrapolated to high frequencies. The correlation function has the advantage that the background detector noise produces a peak at the origin that can be separated from the coupled-core effects.

3. EXPERIMENTAL METHOD

The neutrons in the assembly were detected by two high efficiency BF_3 proportional counters (20th Century Electronics, Ltd. Type 40EB70/50/G). The detector pulses were amplified and discriminated to give pulses of uniform amplitude and width for input to the ratemeters. The ratemeter had a wide frequency response with 0.11 dB attenuation at 200 Hz and 2.2 dB attenuation at 1 kHz. The outputs of the two ratemeters were recorded on magnetic tape at 3.75 inches per second with an AMPEX FR-1300 tape recorder. The tape recorder had 2 dB attenuation at 1 kHz, but the attenuation rapidly increased at higher frequencies.

The data were further filtered before analysis by two 'Rockland' 16-fold resistance-capacitance low-pass filters set at 2 kHz. These filters

produced an attenuation of 0.8 dB at 200 Hz and 18 dB at 1 kHz, and were the most important components determining the frequency response of the whole system.

The cross- and auto-correlograms for 100 time lags were determined with a Hewlett-Packard correlator (Model 3721A). The data were sampled every 666 us for the coupling measurements. The maximum number of samples the correlator could accumulate for each correlogram was 128 x 1024, corresponding to about 87 seconds of data. Many such correlograms were obtained and added together to improve the signal-to-noise ratio.

The random noise present in the data caused the zero time lag peak in auto-correlograms, and the shape of the peak is a measure of the frequency response of the whole system. This frequency response was calculated by combining the responses of the ratemeter, the tape recorder and the low pass filters. The total power frequency response was then Fourier transformed to determine the theoretical correlogram window function. The resulting peak (Figure 3) had the same width and shape as the observed zero time-lag peak on the auto-correlograms, thus confirming that the correct frequency responses were used. The effect of the system frequency response on the observed correlogram is to convolve the ideal correlogram with the window function. The narrowness of the window function means that it only had a significant effect on the zero time-lag peak of the auto-correlograms; the effect on the more slowly varying parts of the correlograms could be ignored.

A calibration signal, consisting of a 20 kHz pulse signal gated by a 100 Hz square wave, was used to check the performance of the system from the discriminator input to the correlator. The amplifications of the two ratemeters were set so that an equal amplitude signal was obtained on the magnetic tape for both channels with the same calibration signal at the discriminator inputs. Auto- and cross-correlograms of each calibration run provided the timing characteristics of the system. The calibration runs showed that the mean sampling rate for the correlogram was 0.667 ms with a maximum deviation of 0.0011 ms. The channel A signal was observed to lag the channel B signal, presumably due to misalignment of the 'read' or 'write' head on the tape recorders, by a mean delay of 82 μs with a maximum observed of 188 μs. Even the extreme value is only 28 per cent of the sampling period and does not significantly affect the slowly varying cross-correlograms.

Pickup from one channel to the other was measured with the calibration

signal input to one discriminator only. A pickup of 0.12 per cent was observed, with a possible upper limit of 0.24 per cent. The cross-correlograms from assemblies M1 and M2 showed a slight excess in the zero time-lag point when compared with the subsequent points. The amount of excess depended on the ratio of correlated to uncorrelated signal but, for these assemblies, the mean was 0.44 per cent.

4. REACTOR ASSEMBLIES

Four coupled-core reactor assemblies were constructed on the Split-table Critical Facility [McCulloch 1972] with the aim of varying the coupling between the cores. The first assembly (M1) was a mockup of Moata with coupled cores, water cooling and a graphite reflector [Marks 1962]. The essential features of this assembly are shown in Figure 4. The assembly had six absorber rods; four of these were safety rods that were out of the assembly during the experiments, and two were control rods used to control the assembly reactivity. Each individual core consisted of six boxes containing the 90 to 93 per cent enriched ^{235}U strips surrounded by polythene. Two different sizes of box were used and the fuel density was lower in the larger boxes (1A, 2A, 1D and 2D).

The differences between the four assemblies are given in Table 1. The most significant change between assemblies M1, M2 and M3 is the increasing separation between the cores. A secondary change was the rearrangement of the fuel so that the higher density boxes were towards the assembly centre line for assemblies M3 and M4.

TABLE 1

CRITICAL FACILITY ASSEMBLIES

Assembly	Spacing	Fuel configuration	Coupling region
M1	450	A	Graphite
M2	600	A	Graphite
M3	800	B	Graphite
M4	450	B	Graphite
M4 (Fe)	450	B	Graphite + Iron

NOTE: Fuel configuration:

A lower density fuel boxes closest to assembly centre line

B higher density fuel boxes closest to assembly centre line

Assembly M4 had the same core separation as M1, but the fuel configuration of M3. Coupling measurements were also taken with steel strips (1.6 mm x 50 mm x 800 mm) added to the assembly M4 coupling region. Each strip fitted into a slot milled into the edge of the 100 mm square graphite blocks which were used to construct the assembly.

Flux scans were made using manganese foils positioned in the assembly. Figure 5 shows neutron flux across assembly M3 for two different control-rod configurations. The marked tilting of the neutron flux evident in these flux scans is made possible by the weak coupling between core tanks.

5. CORRELATION RESULTS

The correlograms were obtained at two sampling rates, 0.666 ms for the coupling analysis and 2.667 ms for the prompt neutron decay constant analysis. The 0.666 ms sampling rate did not provide good determination of the background level for the exponential fit, but it was necessary to show the correlation function behaviour at short time intervals. At larger time lags, the correlation function approaches $\exp(-\alpha|t|)$ where α is the prompt neutron decay constant. The prompt neutron decay constant analysis will be reported separately.

Figure 6 shows the sum of the A-delayed and B-delayed cross-correlograms from the different assemblies normalised to the same exponential asymptote at larger lag times. The effect of weaker coupling is to decrease the correlogram amplitude at shorter time lags. The frequency response of the detection system (Section 3) has very little effect on these curves.

The cross-correlograms of assemblies M1 and M2 can be approximated by the theoretical correlation function derived for the two-node model with no time delay (Equation 8). However, this approximation for the cross-correlograms is not as good for assembly M3, because the time delay for neutrons travelling between the two cores becomes significant at the weaker coupling.

The coupling coefficient was first determined by taking the difference between the auto-correlograms and the cross-correlograms. The A and B auto-correlograms were added to improve the accuracy of the data, as were the A-delay and the B-delay cross-correlograms. For no flux tilt and no time delay between cores, the difference between the auto- and the cross-correlograms should be a single exponential. The single exponential plus a constant background term were fitted using the least-squares method. Figure 7 shows one of the auto- plus and minus cross-correlogram fits for assembly M3. The fit is satisfactory even to times as short as

1.5 ms and the tilts of up to 0.7 (N_1/N_2) observed in assembly M3 did not significantly change the coupling parameter obtained from these fits.

The results of these exponential fits to the correlogram data for each assembly are shown in Table 2. The values of the exponent α_1, the prompt neutron decay constant, were derived from the 2.667 ms sample correlograms, while the exponent α_2 was obtained from the auto-minus cross-correlograms with 0.666 ms sample rate. The coupling coefficient was calculated from these two components using Equation (9).

TABLE 2

THE COUPLING COEFFICIENT AND PROMPT NEUTRON DECAY CONSTANT DETERMINED BY LEAST SQUARES FITS OF EXPONENTIAL FUNCTIONS TO THE CORRELOGRAM DATA

Assembly	α_1	α_2	ε/β	ε
M1	24.9 ± 0.4	341 ± 22	\$6.3 ± 0.4	0.047 ± 0.003
M2	24.4 ± 0.3	223 ± 10	\$4.1 ± 0.2	0.030 ± 0.0013
M3	28.9 ± 0.3	137 ± 7	\$1.9 ± 0.1	0.0138 ± 0.0007
M4	30.8 ± 0.6	398 ± 8	\$6.0 ± 0.2	0.044 ± 0.0014
M4(Fe)	35.8 ± 0.6	344 ± 8	\$4.3 ± 0.14	0.032 ± 0.0010

NOTE: α_1 *determined from 2.667 ms sample correlogram,* $\alpha_1 = \beta/\Lambda$

α_2 *determined from the 0.666 ms sample correlograms by least squares fit to auto-minus cross-correlogram*

$\alpha_2 = (\beta+2\varepsilon)/\Lambda$

$\beta_{eff} = 0.0074$

Data were taken at different power levels, at different detector positions and on different days, but no systematic trend was observed. The errors shown in Table 2 are the standard deviation of the mean from these various experiments.

The effect of flux tilts and time delays between the two cores becomes significant in assembly M3. The measured auto- and cross-correlograms for a high flux tilt (Figure 8) are similar to the theoretical correlograms for a tilted core with time delay (Figure 2).

Because of the difficulty in determining an analytical expression for the cross-correlation function with a fixed time delay, the data were transformed to the frequency domain. A background adjustment was made to B-delayed to make the A-delayed and B-delayed cross-correlograms

equal at zero time lag. This difference, which was less than 2 per cent, is probably due to differences in the digitisation of the two signals in the correlator. The time data were then extrapolated with an exponential function to give a total of 512 'data' points for both positive and negative time lags. A least-squares technique was used to fit the exponential to the data from 50 to 100 time lags in each direction. Although the amplitude and exponent of the exponential function were independent in each direction, the background level was common. A fast Fourier transform program was used to calculate the cross-spectrum from the extrapolated cross-correlogram.

The cross-spectrum of Experiment 6 for assembly M3 is shown in Figure 9 and shows the real component passing through zero at the sink frequency. The magnitude of the imaginary component depends on the flux tilt between the cores. The mean sink frequency from the cross-spectra was (77 ± 4) Hz for assembly M2 and (35.5 ± 1.0) Hz for assembly M3.

The theoretical cross-spectra equation for the two-node one-group model with a fixed time delay (Equation 4) was fitted to the data by the least-squares technique. The assembly reactivity during each experiment was known from the control-rod settings and the coupling between the cores was directly related to the reactivity of each core and the assembly reactivity. The least-squares program optimised the fit by varying five parameters: the reactivity of each core; the time delay between the cores; the prompt neutron decay constant; and an amplitude term. The real and imaginary components of the cross-spectrum were fitted at the same time.

The results from the cross-spectrum fitting program are listed in Table 3. The errors are the standard deviations in the estimates of the means from several different experimental runs but do not include systematic errors. Figure 9 shows one of the cross-spectra obtained for an experiment on assembly M3 together with the theoretical fitted cross-spectrum.

The cross-spectrum power above 100 Hz was very small for all assemblies, and so the effect of the bandpass of the analysis system is negligible. At 100 Hz, the power attenuated by only 4.6 per cent.

TABLE 3

THE COUPLED-CORE PARAMETERS DETERMINED BY THE LEAST-SQUARES FIT OF THE TWO-NODE MODEL TO THE CROSS-SPECTRUM DATA

Assembly	α	Coupling		delay, τ(ms)
		ε/Λ	ε/β	
M1	26.9 ± 0.7	167 ± 14	6.2 ± 0.5	0.06 ± 0.07
M2	26.0 ± 0.6	92 ± 5	3.5 ± 0.2	0.51 ± 0.07
M3	31.2 ± 0.8	45.7 ± 2	1.46 ± 0.08	1.50 ± 0.07
M4	30.2 ± 0.6	175 ± 16	5.8 ± 0.5	(-0.10 ± 0.10)
M4(Fe)	35.8 ± 1.0	160 ± 16	4.5 ± 0.5	(-0.29 ± 0.10)

NOTE: 1. The coupling ε/β was determined from the fitted parameters ε/Λ and α

The derived coupling reactivities for the 450 mm cores are in good agreement with the coupling reactivities obtained by fitting the no time delay model to the difference between the auto- minus cross-correlograms. However, the time delay was significant for assemblies M2 and M3, and this explains the difference between the coupling reactivities measured by the two methods for these assemblies. The cross-spectrum analysis, which includes a time-delay effect, gives the more valid coupling reactivity.

The time delay between the cores increases rapidly as the separation increases. The time delay for the 450 mm separation was too small to be observed in the present experiments, but it was 0.5 ms for the 600 mm separation and 1.5 ms for the 800 mm separation assembly.

6. FLUX TILT

The coupling between the two cores can also be determined by measuring the flux tilt produced by a reactivity difference in the cores. This can be achieved by a sudden reactivity change in one core (*e.g.* a rod drop) and measuring the neutron flux before and after the change, or by measuring a static flux tilt. Rydin *et al.* [1971] used both static and transient flux tilt to measure coupling properties, while Jeffers & Hall [1968] used static flux tilts produced by asymmetric fuel loadings.

A transient flux tilt is analysed using the one-group two-node kinetic Equations (1). Initially, the reactor is critical with individual core reactivities of ρ_1 and ρ_2 and the delayed neutron precursors are assumed to have had time to reach equilibrium. The kinetic equations are

solved for the neutron fluxes after the rod drop when the reactivities of the two cores are $\rho_1-\delta$ and ρ_2. The most convenient solution is found by using Laplace transforms and taking the limit as s, the transform variable, tends to zero giving

$$\int_0^\infty N_1(t)dt = \left(\frac{\Lambda}{\beta} + \Sigma_i \frac{a_i}{\lambda_i}\right) N_1(0) \frac{\beta}{\delta} \left(1 + \frac{\rho_1}{\rho_2}\right) ,$$

$$\int_0^\infty N_2(t)dt = \left(\frac{\Lambda}{\beta} + \Sigma_i \frac{a_i}{\lambda_i}\right) N_2(0) \frac{\beta}{\delta} \left(1 + \frac{\rho_1}{\rho_2} - \frac{\delta}{\rho_2}\right) . \quad ...(10)$$

The delayed neutron values of Keepin [1965] and the experimental Λ/β give

$$\frac{\Lambda}{\beta} + \Sigma_i \frac{a_i}{\lambda_i} = 12.8 \pm 0.2 . \quad ...(11)$$

In the critical reactor the initial reactivities, the coupling coefficient and the initial flux tilt are related by Equation (2).

Define integrals I_1 and I_2 to be

$$I_1 = (0.0781 \pm 0.0012) \int_0^\infty N_1(t)/N_1(0)dt ;$$

$$I_2 = (0.0781 \pm 0.0012) \int_0^\infty N_2(t)/N_2(0)dt .$$

Then substituting from Equations (10), gives

$$I_1 = (\beta/\delta) \left[1 + [N_1(0)/N_2(0)]^2\right] ;$$

$$I_2 = (\beta/\delta) \left[1 + [N_1(0)/N_2(0)]^2 + (\delta/\varepsilon) \left[N_2(0)/N_1(0)\right]\right]. \quad ...(12)$$

Hence $$\varepsilon/\beta = [N_2(0)/N_1(0)]/(I_2-I_1) ;$$

$$\delta/\beta = [1 + [N_1(0)/N_2(0)]^2]/I_1. \quad ...(13)$$

These equations enable the reactivity step and coupling coefficient to be determined from the initial flux tilt and the integrals I_1 and I_2. Note that the integrals involve only the ratio of the neutron flux to the initial neutron flux. The assumption of no external source is reasonable at the pre-drop power, but after the drop the neutron flux falls asymptotically to a mean background source level and a source correction must be made.

Two BF_3 proportional counters (6.3 mm diameter, 20th Century Electronics Ltd. Type 5EB70) were used to detect the neutrons from the two cores. The detectors were placed in graphite stringers beside each core. The power level in the assembly was held steady for at least 15 minutes before control rod H in the west core was released to produce the flux tilt. The data were collected on a Laben 512-channel analyser used in multiscaler mode with a one-second stepping rate. Thirty-two seconds of data were recorded before the drop and 480 seconds of data after the drop. Countrate data from only one detector were recorded in any run, so that exactly the same analysis system could be used for both detectors by a repeat run with the same initial conditions.

A least-squares technique was used to fit an exponential function plus background to the data after 300 seconds in order to determine the background source contribution. This background level was subtracted from all neutron fluxes after the rod drop. The data were also corrected for deadtime losses in the pre-drop countrate.

Rod drops were carried out with the pre-drop fluxes equal in each core, and flux tilts. The relative efficiencies of the two detectors were determined by using them together to determine the flux at the centre of the coupling regions, and then reversing their relative positions. The coupling reactivities determined by the rod-drop method are shown in Table 4.

TABLE 4

COUPLING REACTIVITY FROM FLUX-TILT EXPERIMENTS

Assembly	Static tilt	Rod drop
M1	\$5.6	\$5.12
M2	\$2.9	\$3.49
M3	\$1.4	\$1.49

The movement of the rod changes the flux distribution in each individual core, and so changes the relationship between the detector countrate and the amplitude of the fundamental mode flux distribution in the core.

Manganese foil measurements of flux distributions showed that the relative flux change might be overestimated by as much as six per cent for some rod movements. An effect of this magnitude would cause an increase of more than 20 per cent in the coupling reactivities determined from the rod drops.

Static flux tilts were also measured for different control rod positions. The two-node model relates the change in flux tilt, $\Delta(N_1/N_2)$, to the change in a single core reactivity and the coupling by:

$$\Delta(N_1/N_2) = \Delta(\rho_2)/\varepsilon \ . \qquad \ldots(14)$$

Again, it is difficult to estimate the mean flux change from a change in detector countrates when rod configurations are changed. For assemblies M1 and M2 only a single detector position was used, while for assembly M3 three foils were used in each core. The coupling reactivities determined by this method are also shown in Table 4, but they cannot be regarded as accurate because of the uncertainty of relating the detected counts to the mean flux level in the core. Jeffers & Hall [1968] used 40 gold foils to measure the flux distribution for a static tilt produced by varying the fuel loading in each core. Even they had difficulty determining the average flux in each core because of flux peaking in the moderator (McDonnell & Harris 1972].

The coupling coefficients measured by the flux-tilt methods tend to agree with the results of the correlation experiment, but the difficulty of determining the change in flux distribution limits their accuracy.

7. DISCUSSION

The coupling reactivity and the time delay between cores are principally properties of the graphite coupling region with the fuelled core regions having only a secondary effect. This allows the present results to be compared with the results from other graphite coupled-core reactors.

7.1 Coupling Reactivity

The present coupling reactivities and those obtained for similar reactors are listed in Table 5. The previous results were obtained for reactors with a coupling thickness of 300 mm and about 450 mm.

TABLE 5

MEASUREMENTS OF COUPLING COEFFICIENTS FOR GRAPHITE COUPLING REGIONS

Reactor	Separation (mm)	Coupling		Method	
		$	Δk/k		
URR, Lancashire	300	7.8 ± 0.5*	0.058 ± 0.004	Tilt	(1)
		5.22		Oscillator	(2)
		(5.22)		Correlation	(3)
		6.40 ± 0.17		Pulse	(4)
UFTR, Florida	300	see text		Cross-spectrum	(5)
UTR-10, Iowa	457	see text		Correlation	(6)
UTR-100, London	457	4.7*	0.035	Single-core reactivity	(7)
Argonaut	520	2.5*	0.0183	Fuel worth	(8)
Argonaut	520	2.5 ± 0.2		Oscillator	(9)
LFR Argonaut, Petten	550	2.35 ± 0.05		Correlation	(10)
Argonaut, Karlsruhe	460	3.07		Correlation	(11)
		3.06		Rod drop	(12)
AAEC Critical Facility	450	6.1 ± 0.4	0.045 ± 0.003	Correlation	(13)
	600	3.5 ± 0.2	0.026 ± 0.002	Correlation	
	800	1.46 ± 0.0007	0.0108 ± 0.0007	Correlation	

* *Calculated assuming* $\beta_{eff} = 0.0074$

(1) Jeffers & Hall (1968)
(2) Jeffers & Humphreys (1969)
(3) Humphreys & Jeffers (1970)
(4) McDonnell & Harris (1972)
(5) Boynton & Uhrig (1964)
(6) Hendrickson & Murphy (1968)
(7) Leonidou & Mansfield (1971)
(8) Baldwin (1959)
(9) Kawai (1965)
(10) Dragt (1968)
(11) Seifritz & Albrecht (1969)
(12) Kussmaul (1968)
(13) This report

Four different techniques have been used on the Universities Research Reactor (URR), Lancashire, UK, which has a 300 mm coupling region and the agreement between the results gives confidence that each technique is measuring the same parameter. Each technique has some problems [McDonnell & Harris 1972]; the location of the oscillator close to one detector and the presence of a control arm were not considered in the oscillator

experiment; the difficulty of estimating the mean flux distribution because of flux peaking in the moderator in the flux tilt experiment; and the dependence of coupling on the detector position in the oscillator and pulse experiments [Jeffers 1970]. Humphreys & Jeffers [1970] used the correlation method on the URR reactor and found that the results were consistent with the \$5.22 coupling which was determined by the oscillator experiment.

Boynton & Uhrig [1964] used the phase difference between the auto- and cross-spectrum up to 50 Hz to determine the coupling reactivity of the 300 mm separation University of Florida Training Reactor (UFTR). They analysed their results on the two-node model and, by assuming a thermal neutron wave velocity between the core tanks, obtained a coupling reactivity of 0.126 $\Delta k/k$. However, it will be shown that the thermal neutron wave velocity should not be used with the two-node model. If the time delay between the cores were negligible, their results would give a coupling of about 0.052 $\Delta k/k$ (\$7.2)

Reactors in the second group of Table 5 have graphite coupling regions between 450 and 500 mm. The first is the Iowa State University UTR-10 reactor whose coupling was determined by Hendrickson & Murphy [1968]. They measured the sink frequency and then determined a coupling by assuming the thermal neutron wave velocity between cores, so their coupling, which was 0.068 ± 0.011, cannot be compared with the coupling in Table 5. The sink frequency was very close to that observed by Seifritz & Albrecht [1969], suggesting that the coupling for the UTR-10 would also be close to \$3.0.

Leonidou & Mansfield [1971] measured the subcritical reactivity of one core of the University of London UTR-100 by sub-critical multiplication. The reactivity of the single core was -0.035 $\Delta k/k$ when a cadmium sheet was placed between the cores. The subcritical multiplication method is subject to large errors because the flux distribution usually changes significantly as criticality is approached.

The Argonaut reactors have an annular core with a 610 mm diameter, inner graphite thermal column. Coupled-core measurements were made with a two-slab loading which consisted of fuelled boxes in two groups on opposite sides of the annulus. The separation distance listed is an approximate mean separation between the two slabs, and depends on the number of fuelled boxes. Baldwin [1959] first determined the coupling reactivity of this system by comparing the critical mass for the two-slab system with the critical mass for a single slab. Kawai [1965] measured the coupling reactivity, using the oscillator technique, and determined the subcriticality

of the north and south cores to be \$(1.6 ± 0.2) and \$(4.0 ± 0.4) respectively. Equation (2) then gives a coupling reactivity of \$2.5 ± 0.2. The cross-correlation technique has been used on the Argonaut reactors at Petten and Karlsruhe by Dragt [1968] and Albrecht and Seifritz [1969] respectively.

The URR, UFTR, UTR-10, UTR-100 and the Argonaut reactors have similar fuel assemblies and core tank thicknesses of 150 mm, hence the coupling reactivities should show a systematic trend. The coupling reactivities measured on the AAEC assemblies are significantly larger than those measured on the other graphite reactors (Figure 10). This is due mainly to the narrower core tanks which are 100 mm wide. These core tanks have a higher leakage and allow more neutrons to travel into the graphite reflector thereby increasing the coupling.

The iron poisoning in the coupling region reduced both the neutron generation time and the coupling reactivity. The relative changes calculated from Table 2 are:

$$\delta\Lambda/\Lambda_{M_4} = -0.14 \pm 0.03 ;$$

$$\delta\varepsilon/\varepsilon_{M_4} = -0.27 \pm 0.04 .$$

The coupling reactivity depends only on the neutron balance in the coupling region, whereas the generation time depends on the neutron balance both in the coupling region and in the outer reflectors. Hence it is reasonable that a change of the absorption cross section in the coupling region should have twice as much effect on the coupling reactivity as on the generation time.

7.2 Time Delay between the Cores

Time-delay and sink-frequency measurements have been made on several UTR-type reactors and the results are compared with the present results on Table 6.

The three different techniques were used on the Universities Research Reactor (URR) and they all gave similar values. The correlation experiment observed a first sink frequency at 165 Hz, but then the cross-spectrum passed through zero again at 207 Hz [Humphreys & Jeffers 1969]. Theoretical zero crossings were predicted at 160 Hz and 350 Hz for the time delay of 0.23 ms observed in the oscillator experiment. Probably the background variations produced the second zero crossing and this suggests some uncertainty in the first sink frequency. Humphreys & Jeffers

observed that the measured cross-spectrum was consistent with the oscillator time delay.

TABLE 6

MEASUREMENTS OF TIME LAGS BETWEEN CORES

Reactor	Separation	Material	Sink frequency (Hz)	δt (ms)	Reference
URR	300	Graphite	165	(0.23)	(1)
URR	300	Graphite	(Pulse)	0.33 ± 0.16	(2)
URR	300	Graphite	(Oscillator)	0.23 ± 0.02	(3)
UTR-10	457	Graphite	115 ± 5		(4)
Karlsruhe	~460	Graphite	116 ± 8	0.28	(5)
AAEC	600	Graphite	77 ± 4	0.51 ± 0.07	(6)
	800	Graphite	35.5 ± 0.9	1.50 ± 0.07	(6)

(1) Humphreys & Jeffers (1970)
(2) McDonnell & Harris (1972)
(3) Jeffers & Humphreys (1969)
(4) Hendrickson & Murphy (1968)
(5) Seifritz & Albrecht (1968)
(6) This report.

Hendrickson & Murphy [1970] observed the sink frequency of the Iowa UTR-10, but they did not determine a delay time because they did not know the coupling reactivity. However, their sink frequency is almost exactly equal to that measured by Seifritz & Albrecht [1968] on the Argonaut reactor at Karlsruhe which has a similar separation width. Seifritz & Albrecht found that the mean time delay between cores, which was determined from their sink frequency, was insensitive to the time delay function p(t) used.

The delay times observed on the AAEC assemblies are longer than those observed elsewhere because of the greater separation distance. The two-node model of the reactor separates the time delay between the two cores from the response function of the individual core. At the sink frequency, the total phase lag (*i.e.* the sum of the phase lag due to the time for a disturbance to travel from one core to the other), plus the phase lag due to the single core response function, is equal to 90 degrees. In the range of the observed sink frequencies, the response function phase lag is of the order of 70 to 80 degrees.

Nagy & Danofsky [1970] used a two-energy group, one-dimensional modal analysis to predict the behaviour of the sink frequency with core separation. The two fuel regions were 150 mm thick and were modelled on

the Argonaut reactor, but they do not quote the axial buckling used or the reactivity coupling. They predicted sink frequencies of 20 Hz at 800 mm, 45 Hz at 600 mm and 90 Hz at 450 mm. These values agree reasonably well with the observed values.

The time delays determined from the cross-spectra and the two-node model are much shorter than would be expected if the disturbance travelled with the thermal neutron wave velocity between the two cores. Seifritz & Albrecht [1968] note that the estimates of the mean time delay from using thermal neutron waves can be too long by a factor of ten or more for their Argonaut results.

In a block of graphite of cross section 0.6 metres x 1.6 metres, the thermal neutron wave velocity for a one-group diffusion model is 140 m s^{-1} at 50 rad s^{-1} and increases to 170 m s^{-1} at 400 rad s^{-1}. Hence, for a 0.6 m graphite thickness the transit times would be 4.3 ms to 3.5 ms, while for 0.8 m thickness the times are 5.7 ms to 4.7 ms. The mean thermal time delay of 2.82 ± 0.26 ms for the UTR-100 reactor (457 mm separation), measured by pulsed neutron techniques, is consistent with the thermal wave velocity [Leonidou & Mansfield 1971; Leonidou 1972]. The disturbance will travel much faster than the thermal neutron wave for core separation less than the slowing down distance (187 mm for graphite), but as the separation increases most of the neutrons will become thermalised well before reaching the second core, and the time lag would be expected to approach that of a thermal neutron wave.

The use of the two-node model to describe the reactor is inconsistent with using a neutron wave velocity in the coupling region. The two-node model is derived from the time-dependent transport equation by dividing the reactor into two interacting cores and assuming that neutron disturbances travelling between the cores have a time delay function, but that disturbances are propagated instantaneously throughout each individual core. These assumptions lead to the point reactor kinetics equation for describing the response function of each core. Each core consists of a fuelled region and a reflector which includes part or all of the coupling region. It is thus not valid to take the coupling region as a separate entity and use the neutron wave velocity to determine a lag time. Probably the neutron wave velocity is more closely related to the total phase lag between the two cores, *i.e.* the sum of the lag time on the two-node model plus the response function phase lag.

If the neutron wave has a velocity of 150 m s^{-1}, then the frequency

that gives a phase shift of 90° in travelling between the two cores is 125 Hz for 300 mm, 83 Hz for 450 mm, 62 Hz for 600 mm and 47 Hz for 800 mm. These frequencies are similar to the sink frequencies observed for graphite coupling regions and the agreement could be improved by a more precise modelling of the system. However, the important point is that the neutron disturbance can travel with the thermal neutron wave velocity between the cores, even though the relevant time lags for use with the two-node model are considerably shorter than that.

8. CONCLUSION

The two-node model of the coupled core reactor has been found adequate to understand the kinetic behaviour observed on these assemblies. The coupling reactivities observed were stronger than expected from extrapolating the results of the UTR reactors, but the discrepancy is due to the differences in geometry.

The effect of time delays between the two cores was observed for the 600 mm and 800 mm core separation. The use of a fixed time delay in the two-node, one-group model was sufficient to fit the observed cross-spectra. However, the two-node time delay measured cannot be directly compared with the thermal neutron wave velocity, although this time delay is a useful parameter to characterise the reactor.

9. ACKNOWLEDGEMENTS

The author thanks Mr. R.B. Knott for his help with this experiment, Mr. J.W. Connolly for designing the first assembly, and staff and operators of the AAEC Split-table Critical Facility for their technical expertise.

10. REFERENCES

Albrecht, R.W. & Seifritz, W. [1968] - Fundamental properties of the coherence function in a symmetrical two-node system. Nukleonik, 11:143-148.

Baldwin, G.C. [1959] - Kinetics of a reactor composed of two loosely coupled cores. Nucl. Sci. Eng., 6:320-327.

Boynton, A.R. & Uhrig, R.E. [1964] - Evaluation of two-region-reactor parameters by random noise measurements. Nucl. Sci. Eng., 18:220-229.

Danofsky, R.A. [1969] - A space-dependent reactor-noise formulation utilising modal expansions. Nucl. Sci. Eng., 36:28-38.

Dragt, J.B. [1968] - Reactor noise; a study of neutronic fluctuations in low-power nuclear reactors, with special emphasis on accurate time-domain analysis RCN-101, Reactor Centrum Nederland.

Ebert, D.D. & Gallaher, L.J. [1971] - An analytic solution of the space-dependent coherence function. Trans. Am. Nucl. Soc., 14:195-196.

Hendrickson, R.A. & Murphy, G. [1968] - Cross-spectral density measurements in a coupled-core reactor. Nucl. Sci. Eng., 31:215-221.

Humphreys, E. & Jeffers, D.E. [1970] - Spatially dependent noise measurements in a two-zone reactor. Atomkernenergie, 16:132-134.

Jeffers, D.E. & Hall, K. [1968] - Flux tilting in a two-zone reactor. Nucl. Sci. Eng., 31:358-359.

Jeffers, D.E. & Humphreys, E. [1969] - Transfer function measurements in a two-zone reactor. Nukleonik, 12:284-286.

Jeffers, D.E. [1970] - Spatial transfer functions of a two-core reactor. Atomkernenergie, 16:129-131.

Kawai, T. [1965] - Coupled reactor kinetics (1). Transfer function measurements of a coupled reactor. J. Nucl. Sci. Technol., 2:245-250.

Keepin, G.R. [1965] - Physics of Nuclear Kinetics. Addison-Wesley Publishing Co., Massachusetts.

Kussmaul, G. [1968] - Theroetische und experimentelle Untersuchungen zum Zweipunktreaktor. Thesis, University of Karlsruhe. Quoted by Seifritz & Albrecht [1968].

Leonidou, D.J. & Mansfield, W.K. [1971] - Estimation of the coupling coefficient at various subcritical levels of a symmetrical two-core reactor. J. Inst. Nucl. Eng., 12:171-175.

Leonidou, D.J. [1972] - Dependence of propagation phenomena on the reactivity of a subcritical assembly. Atomkernenergie, 19:11-13.

Marks, A.P. [1962] - Moata Reactor. At. Energy Aust., 5 (4) 9-21.

McCulloch, D.B. [1972] - The Critical Facility. At. Energy Aust. 15 (4) 2-14.

McDonnell, F.R.N. & Harris, M.J. [1972] - Pulsed-source experiments in a reflected coupled-core reactor: II - Core coupling measurements. J. Nucl. Energy, 26:129-140.

Nagy, M.E. & Danofsky, R.A. [1970] - Cross-spectral-density sink frequency behaviour for coupled-core Argonaut reactors. Nucl. Sci. Eng., 42:419-421.

Rydin, R.A., Burke, J.A., Moore, W.E. & Seeman, K.W. [1971] - Noise and transient kinetics experiments and calculations for loosely coupled cores. Nucl. Sci. Eng., 46:179-196.

Seifritz, W. & Albrecht, R.W. [1968] - Measurement and analysis of the coupled core coherence function in a two-node symmetrical reactor. Nukleonik 11:149-154.

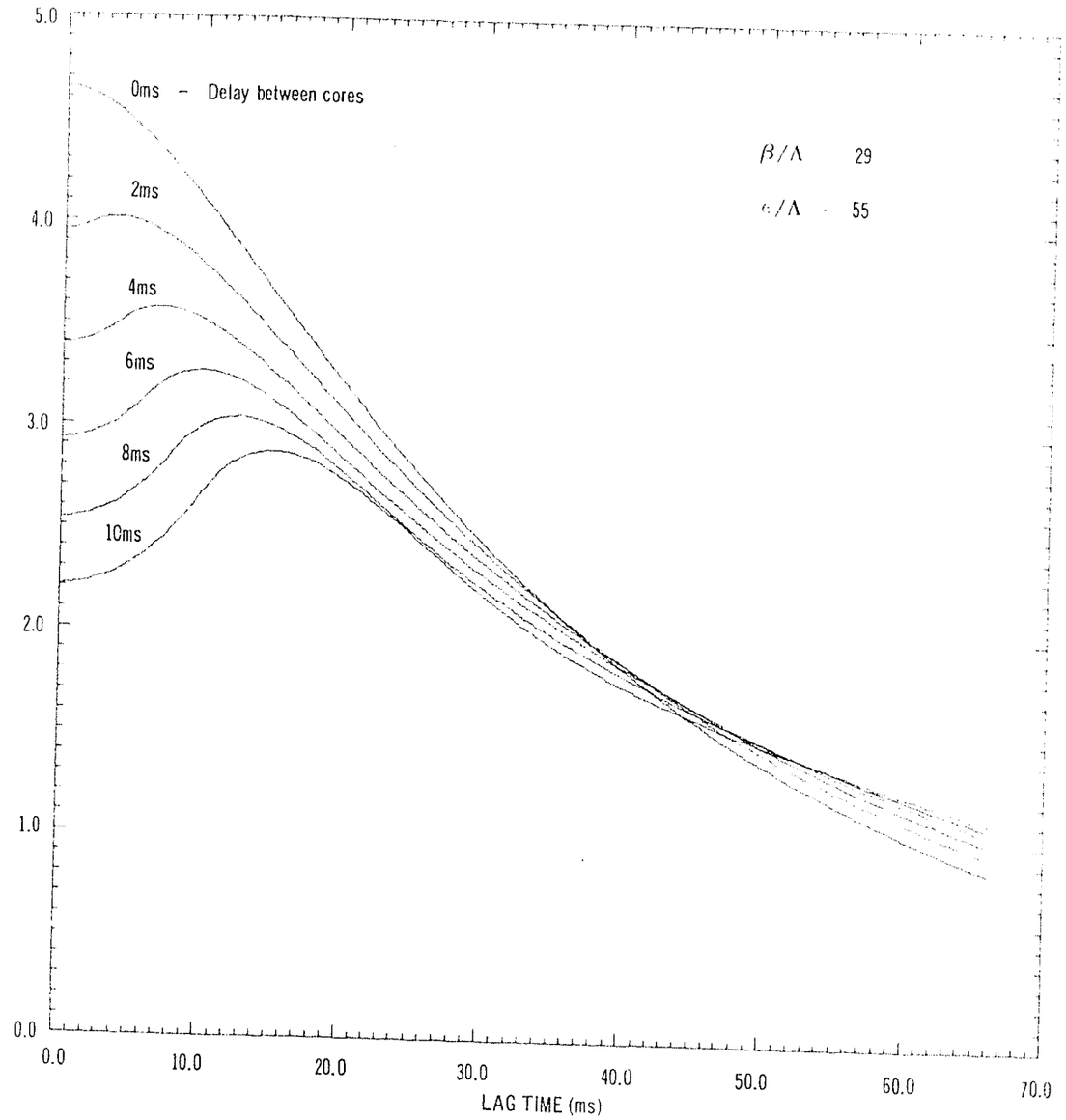

FIGURE 1. THEORETICAL CROSS-CORRELATION FUNCTIONS FOR A COUPLED-CORE REACTOR WITH VARIOUS TIME DELAYS BETWEEN CORES

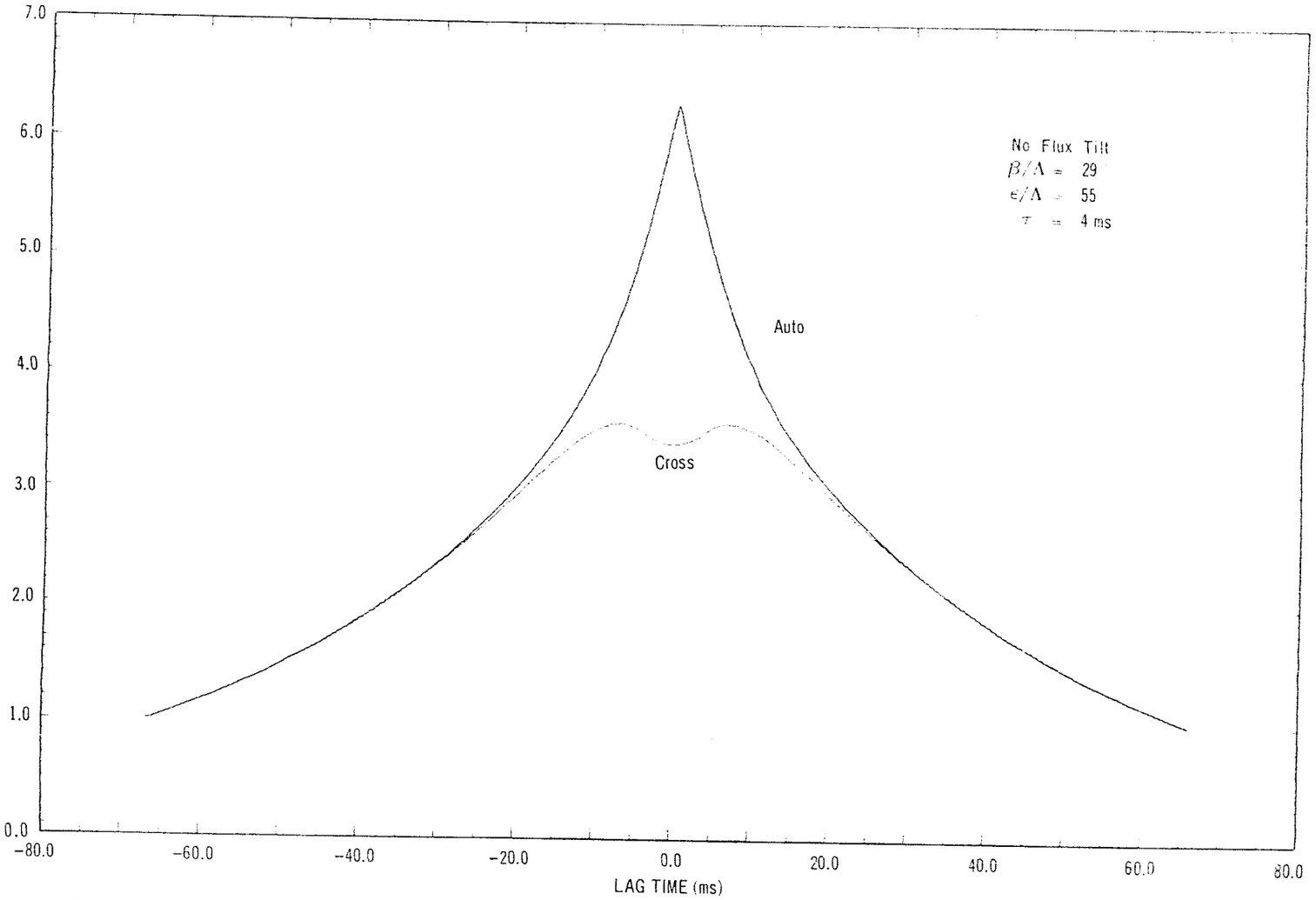

FIGURE 2(a) AUTO- AND CROSS-CORRELATION FUNCTIONS FOR A DELAY OF 4 ms BETWEEN CORES WITHOUT FLUX TILTING

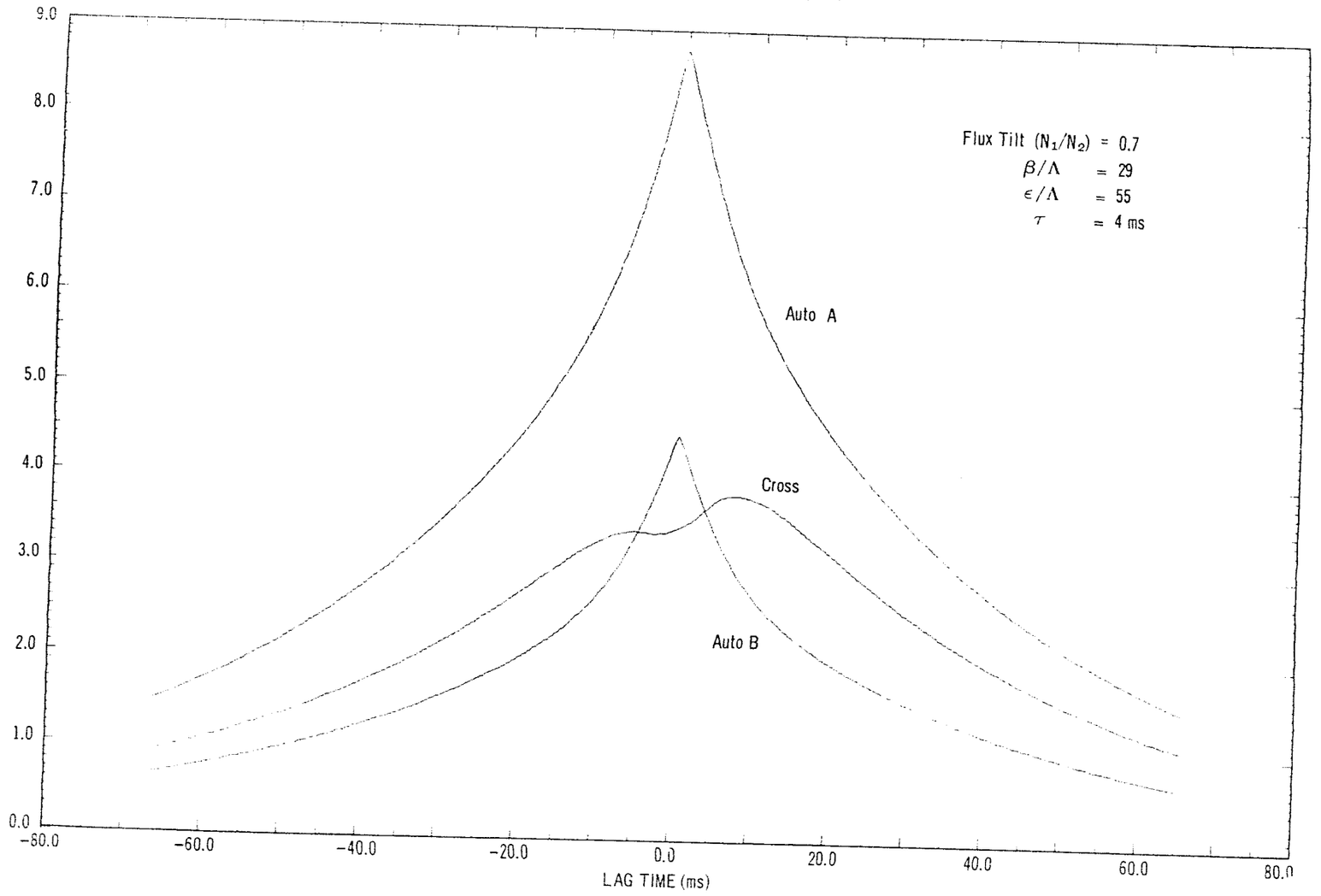

FIGURE 2(b) AUTO- AND CROSS-CORRELATION FUNCTIONS FOR A DELAY OF 4 ms BETWEEN CORES WITH FLUX TILTING

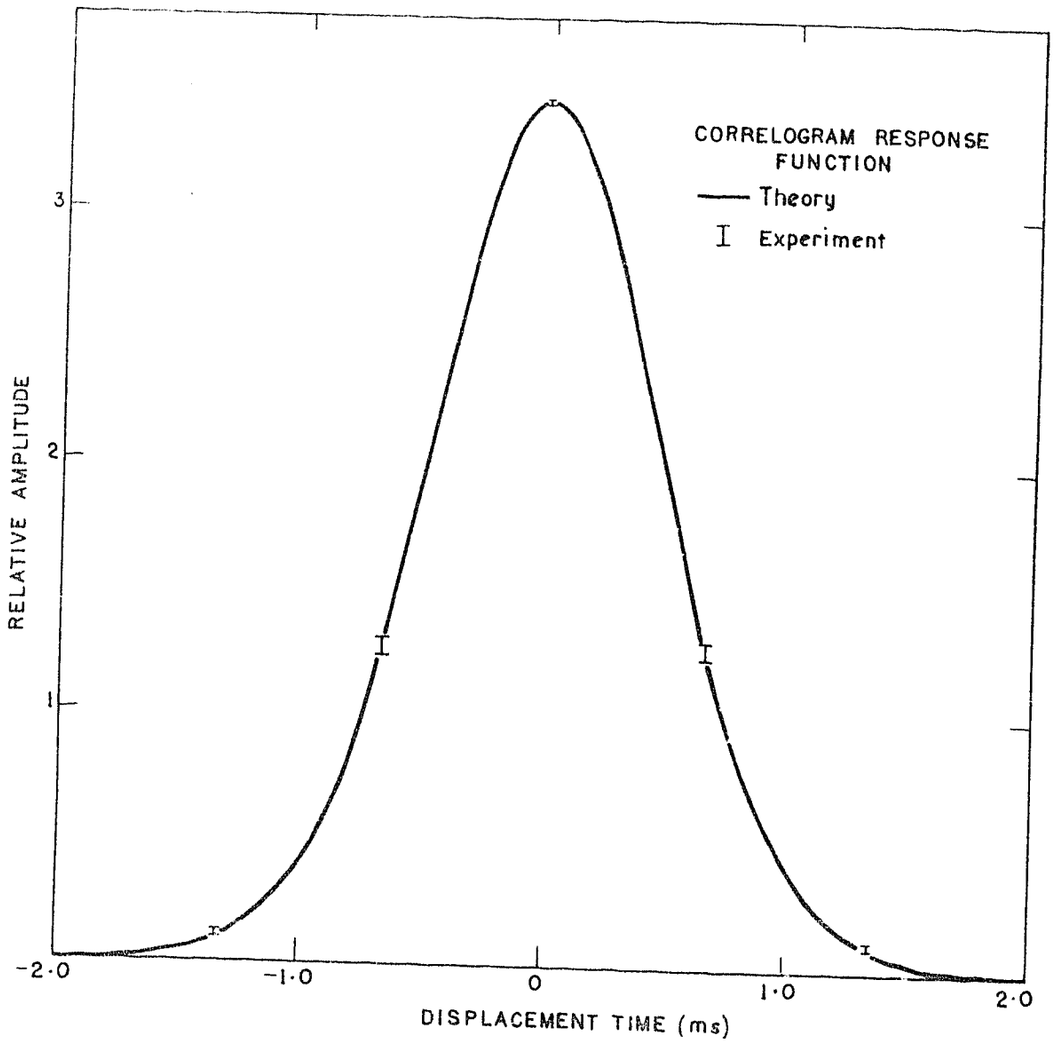

FIGURE 3. CORRELOGRAM WINDOW FUNCTION FOR 0.666 ms CORRELOGRAMS

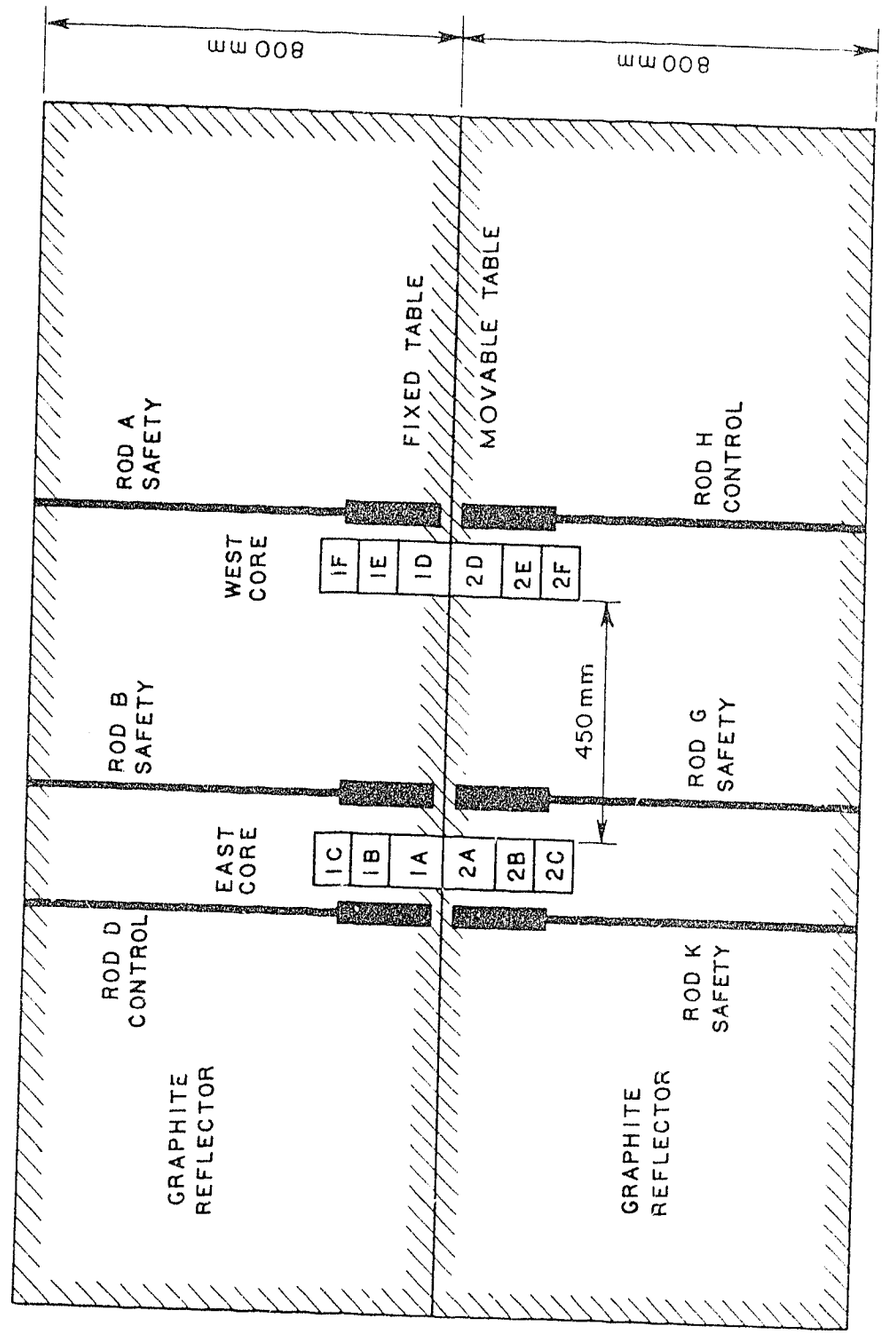

FIGURE 4(a) TOP VIEW OF ASSEMBLY M1, WITH 450 mm COUPLING REGION

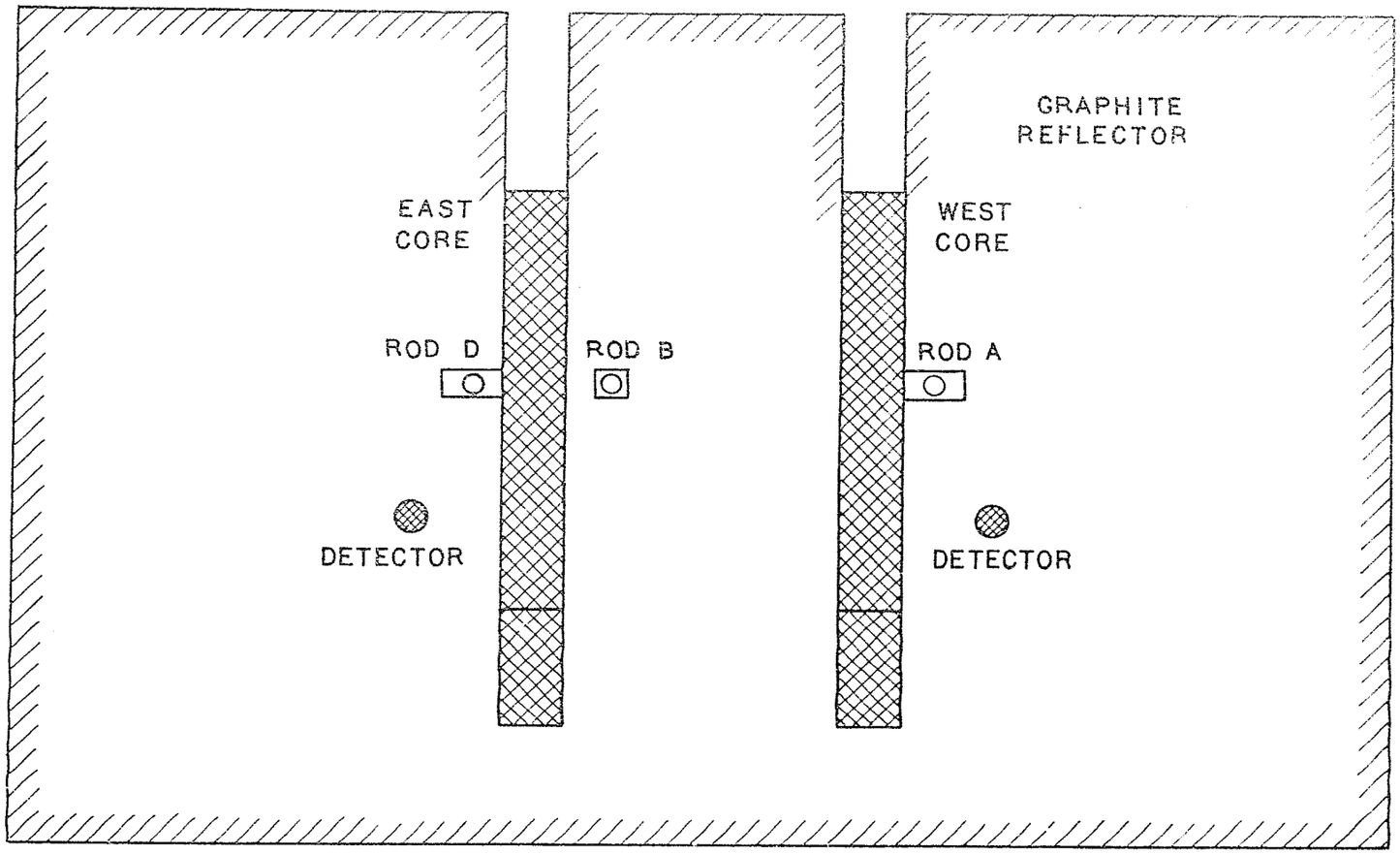

FIGURE 4(b) FRONT VIEW OF ASSEMBLY M1 SHOWING THE CORRELATION DETECTOR

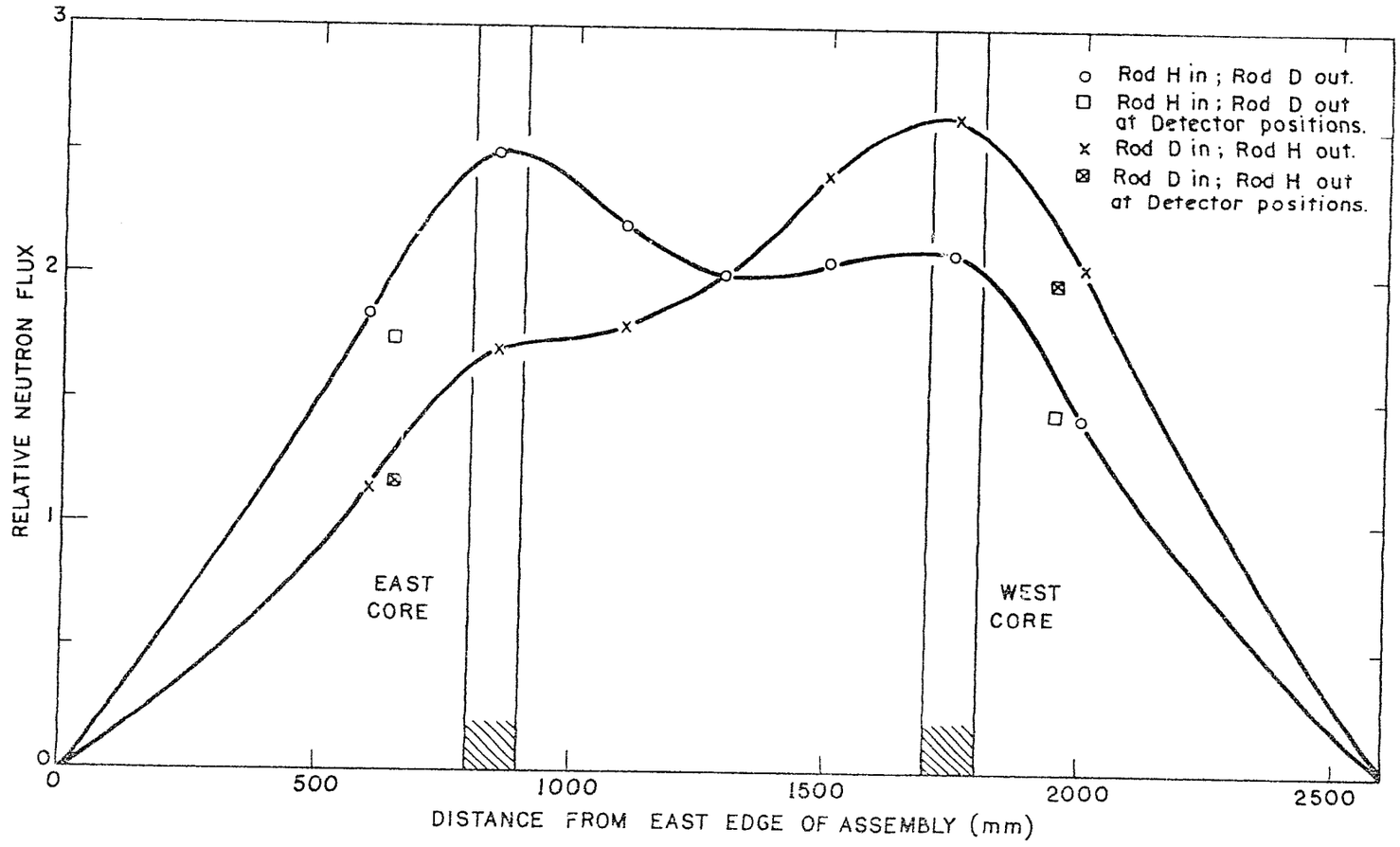

FIGURE 5. FLUX SCANS ACROSS ASSEMBLY M3 AT A HEIGHT OF 700 mm FOR TWO DIFFERENT CONTROL ROD CONFIGURATIONS

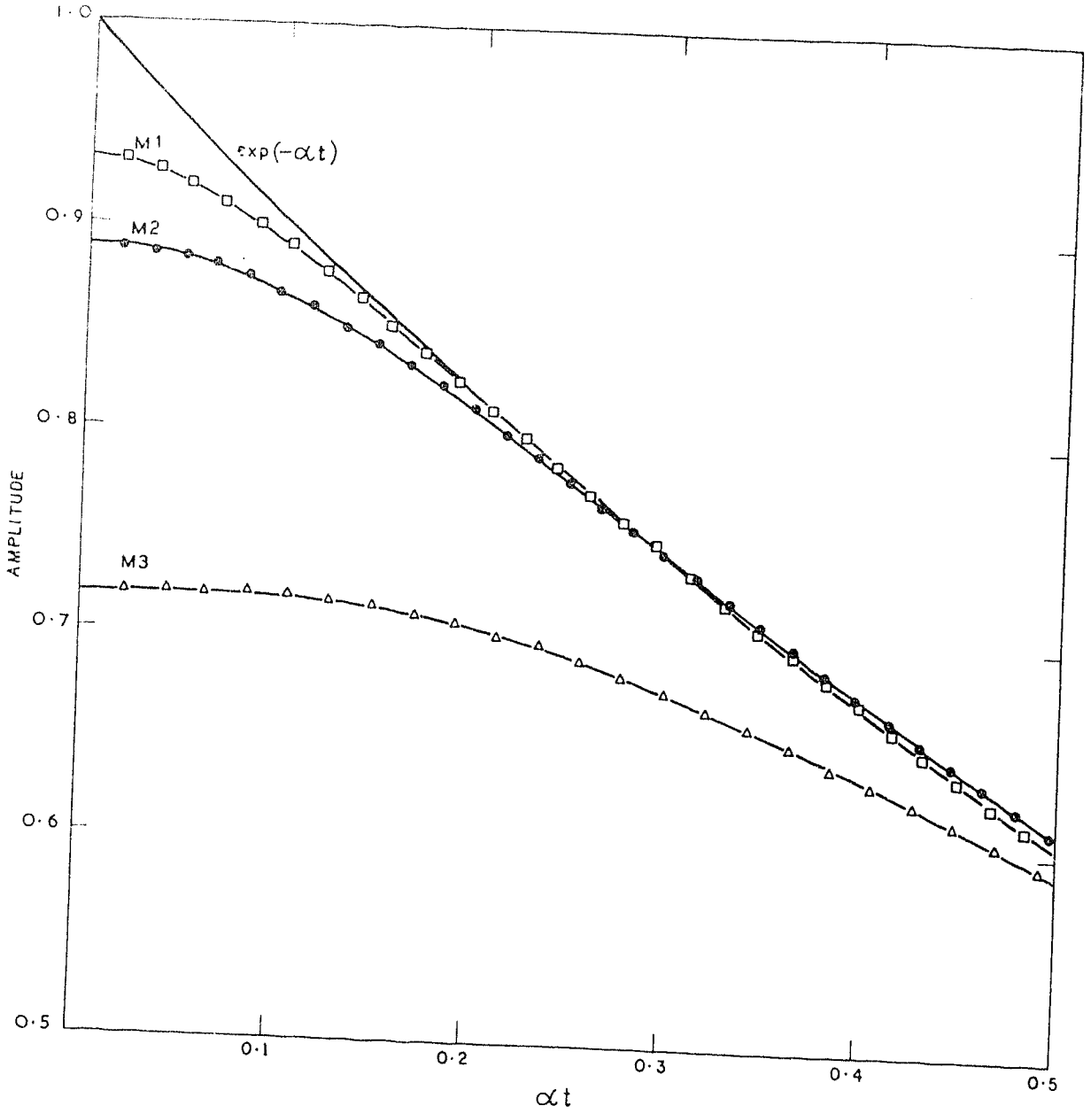

FIGURE 6. CROSS-CORRELOGRAMS FOR ASSEMBLIES M1, M2 AND M3 SCALED TO HAVE THE SAME EXPONENTIAL ASYMPTOTES

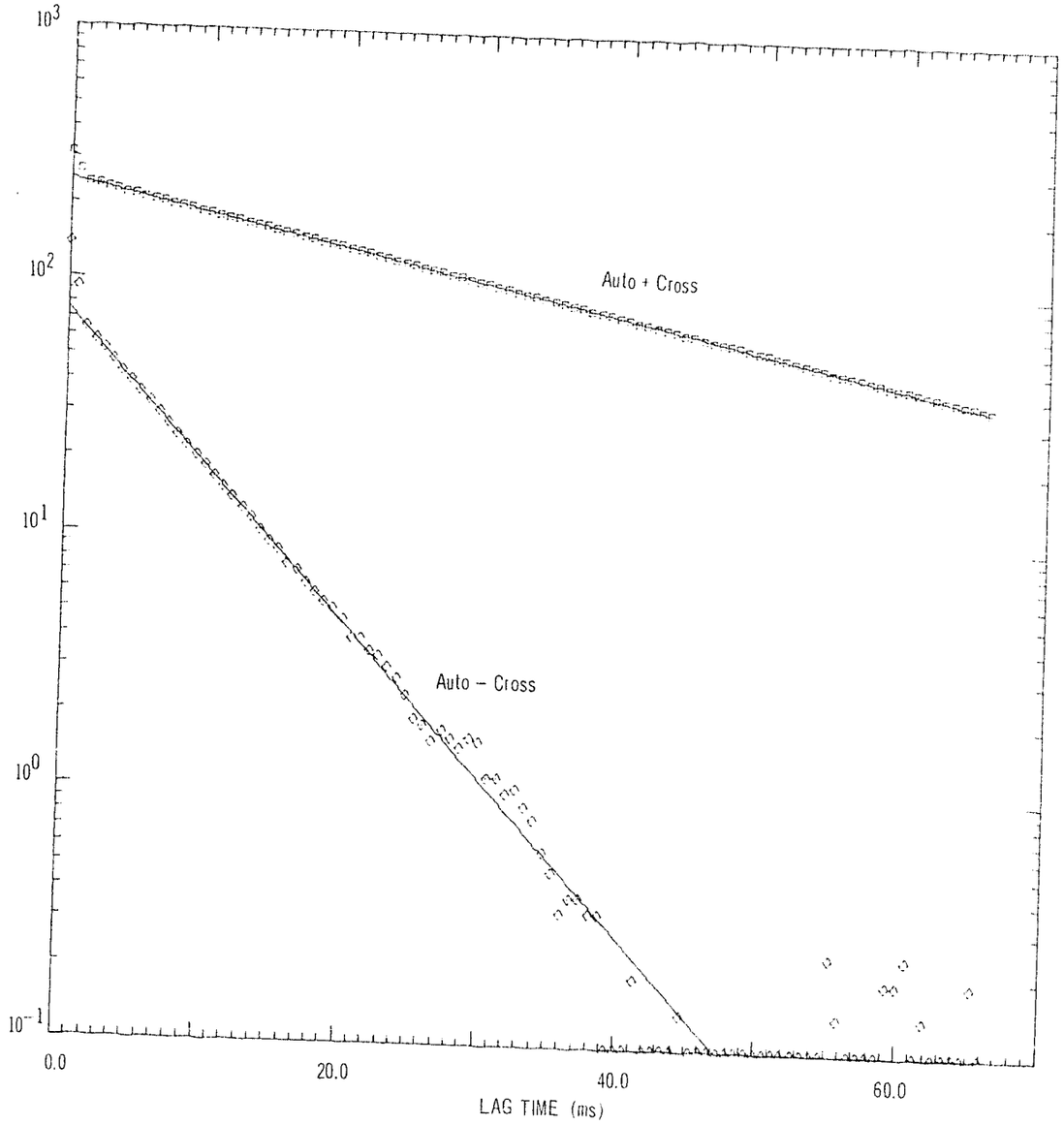

FIGURE 7. PLOTS OF BOTH THE SUM AND DIFFERENCE OF AUTO- AND CROSS-CORRELOGRAMS FOR AN EXPERIMENT ON ASSEMBLY M3. THE LEAST SQUARES FITS TO AN EXPONENTIAL FUNCTION ARE SHOWN. A BACKGROUND COMPONENT HAS BEEN SUBTRACTED.

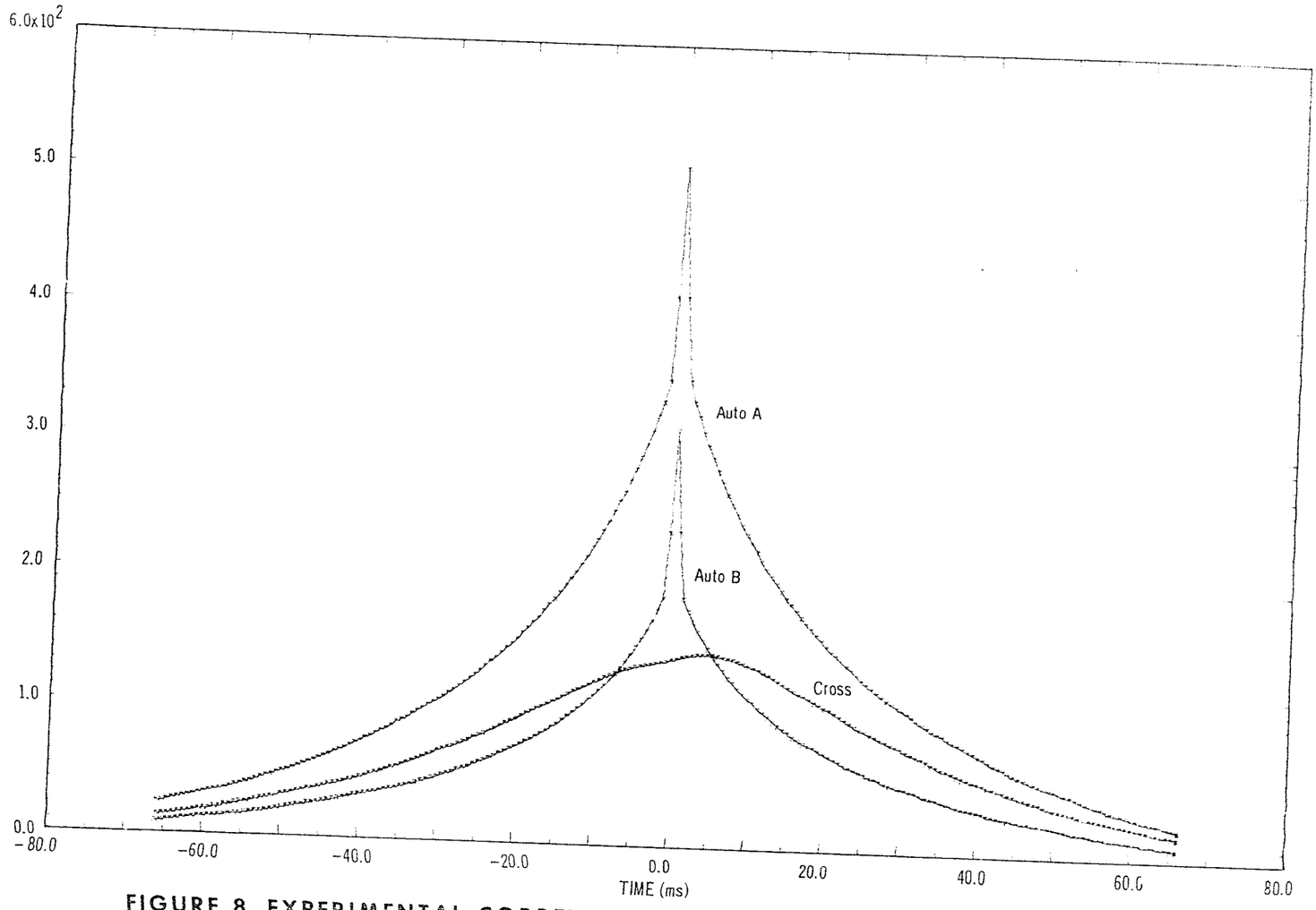

FIGURE 8. EXPERIMENTAL CORRELOGRAMS FROM ASSEMBLY M3 SHOWING THE EFFECT OF A FLUX TILT

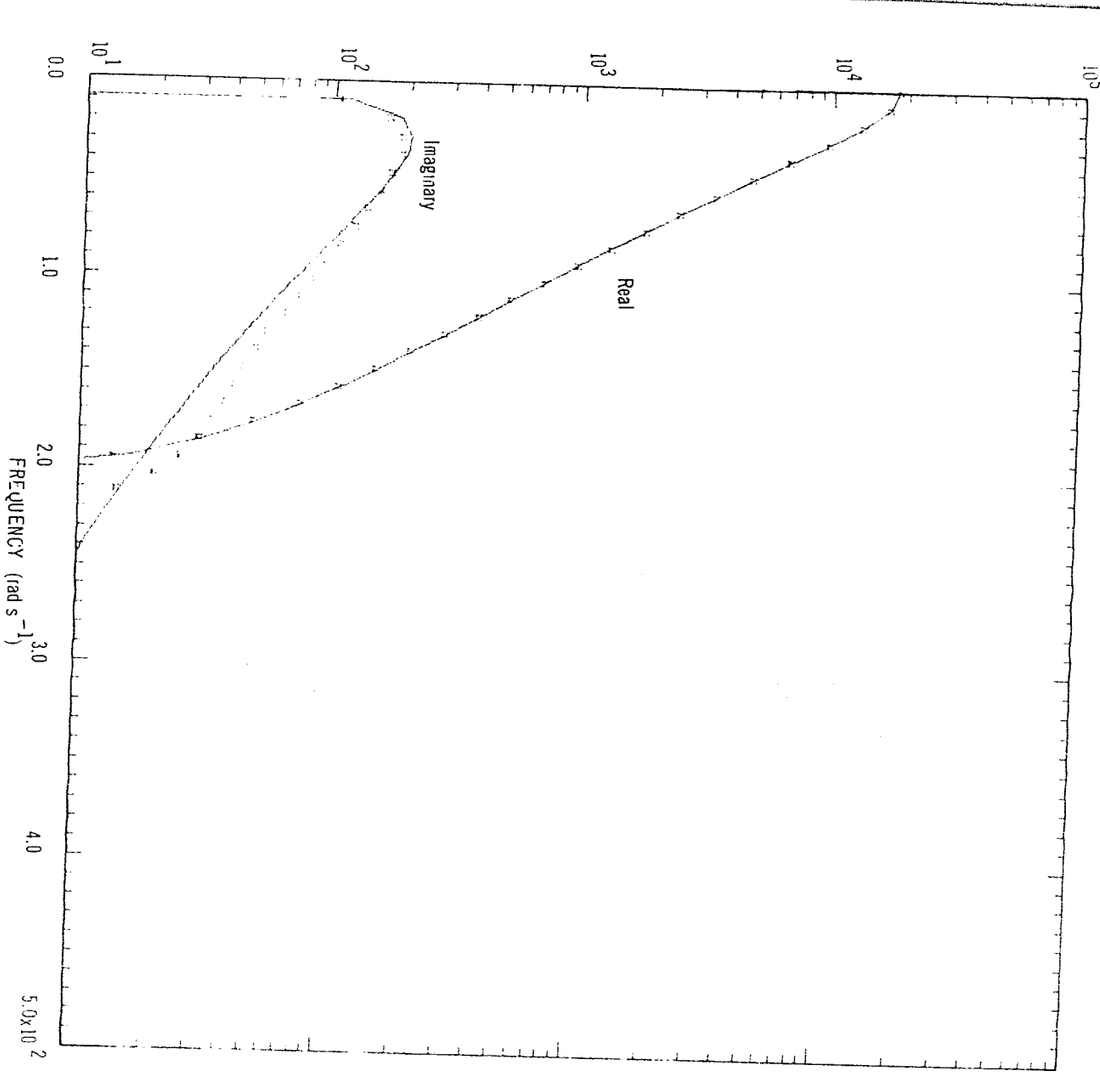

FIGURE 9(a) CROSS-SPECTRUM COMPONENTS FOR EXPERIMENT 6, ASSEMBLY M3 SHOWING THE TWO-NODE FIT (UNBROKEN LINE) TO THE EXPERIMENTAL DATA POINTS

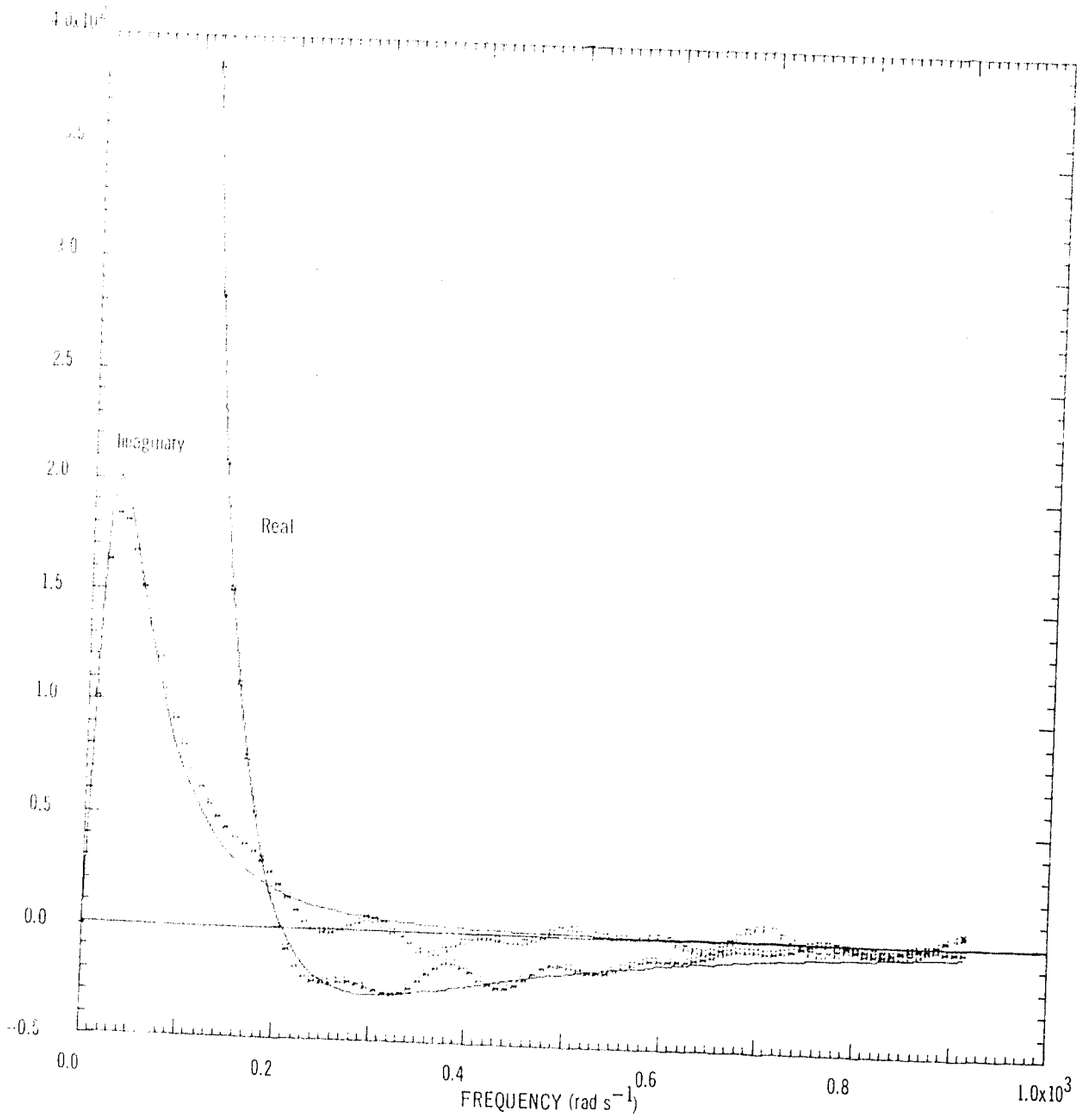

FIGURE 9(b) CROSS-SPECTRUM COMPONENTS AT HIGHER FREQUENCIES (EXPERIMENTAL POINTS AS DOTS) SHOWING THE SINK FREQUENCY AT 203 rad s -1 THE LINE IS THE THEORETICAL TWO-NODE MODEL FIT TO THE DATA

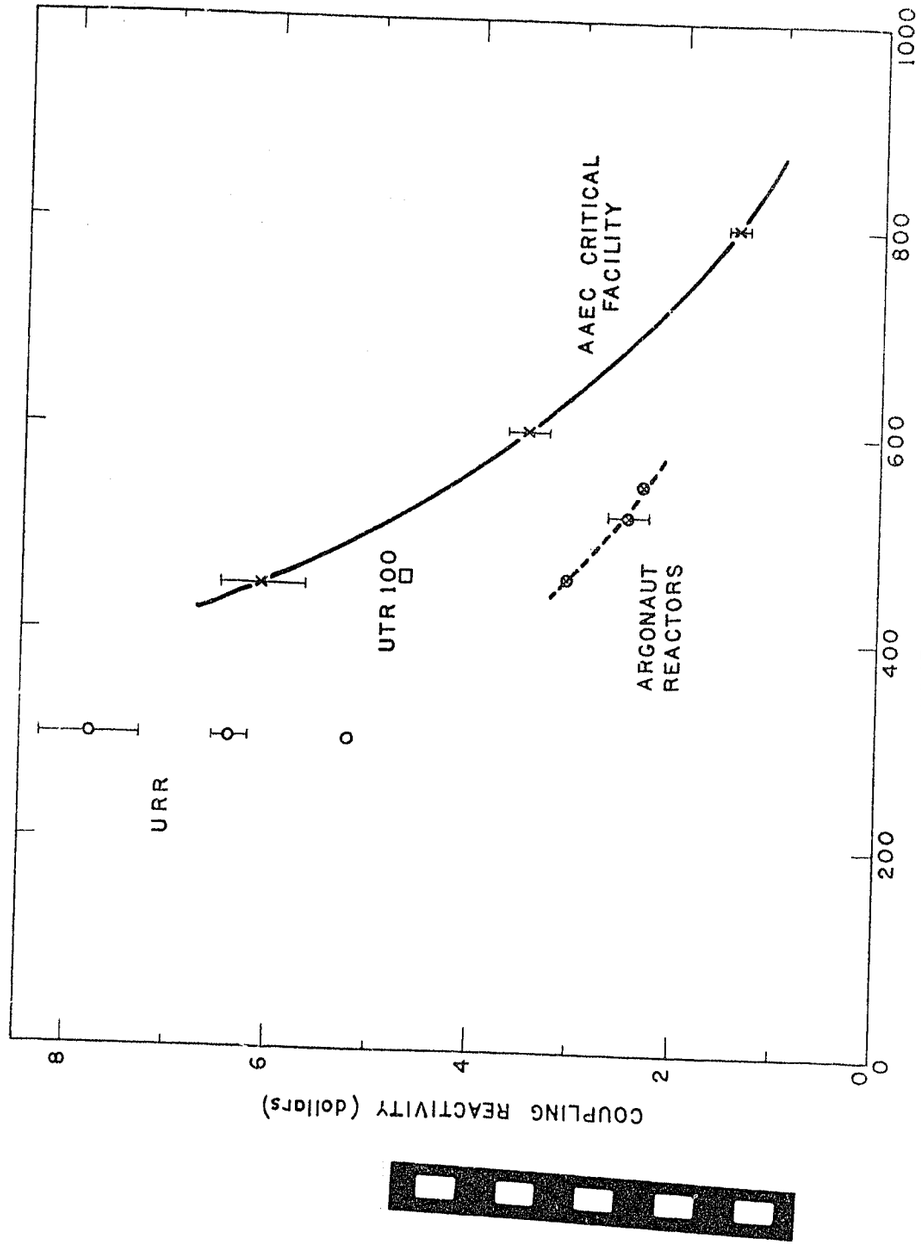

FIGURE 10. COUPLING REACTIVITIES OF THE AAEC ASSEMBLIES COMPARED WITH THE RESULTS FOR OTHER GRAPHITE COUPLED REACTORS